DV-67-006
Copy No. 2

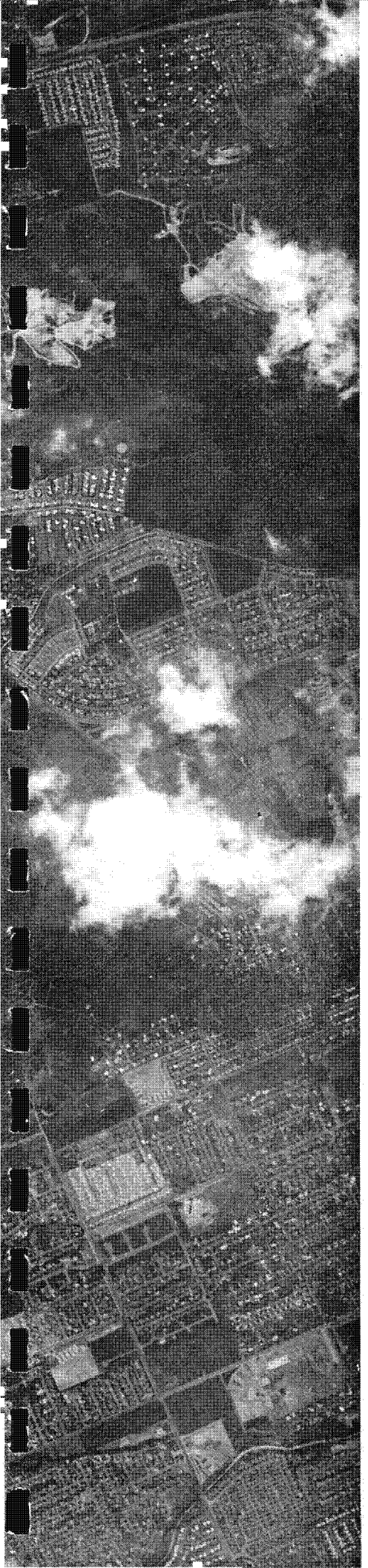

TECHNICAL REPORT

REAL SCENE VIDICON FOCUS SENSOR

26 MAY 1967

Itek

ITEK CORPORATION LEXINGTON 73, MASSACHUSETTS

SPG-67-055

~~SECRET~~

~~SECRET~~

CONTENTS

FIGURES

TABLES

~~SECRET~~

~~SECRET~~

1. GENERAL ANALYSIS—REAL SCENE FOCUS SENSING

1.1 FUNDAMENTAL PROBLEM OF REAL SCENE FOCUS SENSING

1.1.1 Basic Considerations

The general problem of real scene focus sensing can be specified by any real scene object, a lens whose condition of focus (defocus) is to be sensed, and a finite size image of the object through the lens. The first consideration is to determine which characteristics of the image are sensitive to lens defocus, which of these characteristics apply to any and all scenes, and which of thse characteristics are most sensitive. The second basic consideration is to determine how these most sensitive characteristics can be monitored or measured in a feasible electromechanical system.

Any characteristic useful for automatic focusing must be general enough to apply to any real scene and its image. Therefore, one should be cautious in attempting to develop a focus sensor analysis based on artificial scenes such as bar patterns, sinusoidal patterns, sharp edges, or point sources. However, these patterns can be used as specific examples to verify a general theory, since they lend themselves to simple mathematical analysis.

1.1.2 Consideration of Best Focus and Defocus Conditions

Among the first steps in an analysis of real scene focus sensing are to consider the effects of lens defocus on an image and to explain what is implied by the term "best focus." In general, defocus effects on an image comprise qualitative measures such as resolution, spurious resolution, contrast, and detail degradation. These criteria lend themselves to quantitative definition for simple pattern objects, but they cannot be rigorously defined for a real scene as an object.

One way to consider a defocused image is to take the image spread function of a point source (impulse) as a function of defocus. Then each point in the scene image is, by superposition, the sum of all the spread functions of each incremental point in the object scene. Therefore, the defocused image is built up point by point, and each point is evaluated by the superposition integral. This process could alternatively be described by considering the defocused image as equal to the two-dimensional spatial convolution of the object scene with the defocused point source spread function. This convolution technique is one method whereby a defocused image can in theory be derived from a given lens defocus spread function (impulse response). However, for each scene, a separate convolution calculation must be made, and this is indeed a complicated procedure.

A more convenient method of specifying the image as a function of defocus is to consider a spatial frequency domain approach. Here the lens optical transfer function, $\tau(n_x, n_y)$, and its variation with defocus are considered. The scene is characterized by its spatial frequency spectrum, $O(n_x, n_y)$, which is the two-dimensional Fourier transform of the intensity distribution, $o(x, y)$, and n is the spatial frequency in cycles per millimeter.

$$O(n_x, n_y) = \int_{-\infty}^{+\infty} \int_{-\infty}^{+\infty} o(x, y) \exp\left[-j2\pi(n_x x + n_y y)\right] dx\, dy$$

The resulting image is then specified by its frequency spectrum

$$I(n_x, n_y) = O(n_x, n_y)\tau(n_x, n_y)$$

This spatial frequency domain approach to specifying focus is exact for any particular lens considered and gives more insight into the defocusing problem than does the space domain approach. We first consider the modulation transfer function (MTF) variation with defocus, where $|\tau(n_x, n_y)|$ is designated as the MTF. For example, Fig. 1-1 is a plot of the MTF for the diffraction limited, perfect lens case. Spatial frequency has been normalized to the lens cutoff frequency, $n_c = 1/\lambda(f/no.)$, where λ is the wavelength of the light used. In this case, the best focus is the paraxial focus position and corresponds to MTF(0) which is maximum for any frequency, n. For the perfect lens, this is the accepted definition of best focus whereby $|\tau_0| \geq |\tau_k|$ for any n, and the subscripts 0 and k refer to best focus and defocus, respectively.

It should be noted that all the general considerations that follow apply to circular aperture, narrow field angle lenses that can be characterized by an on-axis, circularly symmetric $\tau(n)$. For the case of an imperfect lens, i.e., a lens with finite aberrations, it is required that best focus be exactly defined for any focus sensor analysis. The definition that is to be used is $|\tau_0(n)| \geq |\tau_k(n)|$ or $(MTF)_0 \geq (MTF)_k$ for any frequency, n. The notation $(MTF)_0$ corresponds to a particular focal position which, for the nonperfect lens, is other than the paraxial focus. For small aberrations, this definition corresponds to the focal position obtained when the optimum balanced, fifth-order spherical aberration criterion* is used. It also corresponds to the diffraction focus position where the Strehl intensity is maximized. This follows from the fact that the Strehl intensity or maximum intensity of a point source image, S(0, 0), is equal to the volume under the surface formed by $\tau_0(n_x, n_y)$. This is shown by taking the inverse Fourier transform relationship between $\tau(n_x, n_y)$ and the point source spread function S(x, y).

$$S(0, 0) = \int_{-\infty}^{+\infty} \int_{-\infty}^{+\infty} \tau(n_x, n_y)\, dn_x\, dn_y$$

With this best focus definition for optical systems of interest, we now proceed to consider the characteristics of the image that can be used to sense focus. The optical systems of interest in this case are high quality lenses with small aberrations, narrow field angles, and MTF's that approach those of diffraction limited perfect lenses. The image now is specified in terms of its spatial frequency spectrum, $I(n_x, n_y)$, and its variation with focal position is specified by the MTF as a function of defocus (see Fig. 1-1).

1.1.3 Image Sensitivity to Defocus

Without reference to any particular scene, the effect of defocusing on the image's spatial frequency content can be observed by noting the variation of the lens MTF with defocus, as shown

* R. Barakat, J. Opt. Soc. Am., 51(1):38 (1964).

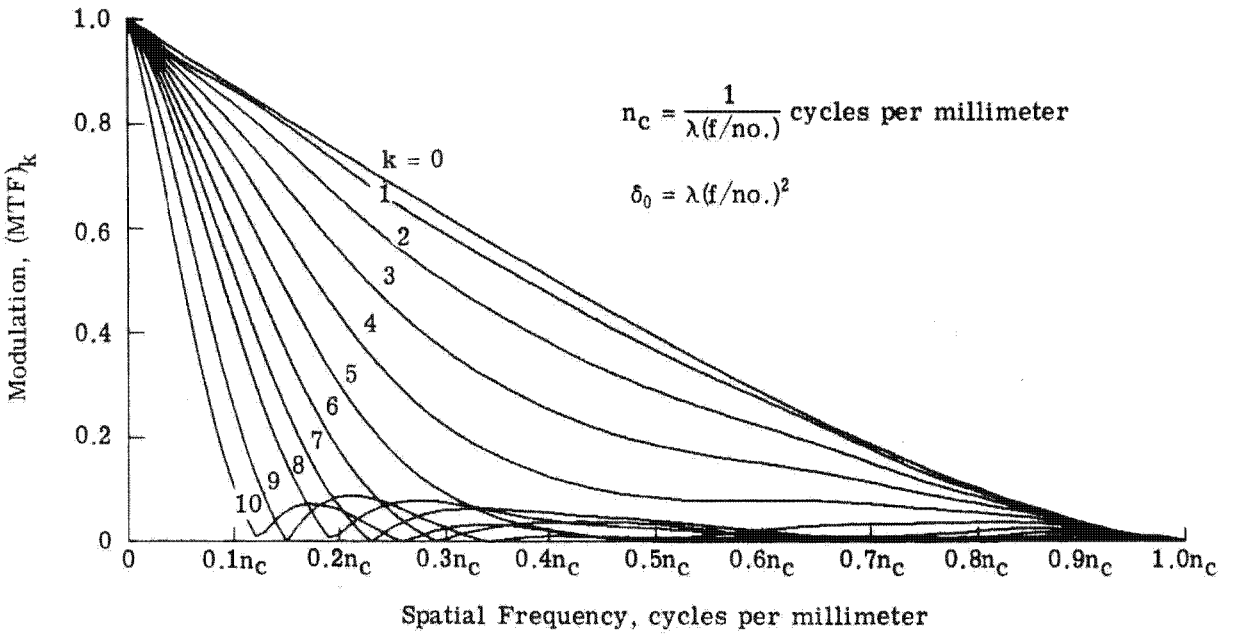

Fig. 1-1 — MTF of diffraction limited, perfect lens versus defocusing, $\pm k\delta_0$ (n_c = lens cutoff frequency, δ_0 = Rayleigh depth of focus, and k is an integer)

in Fig. 1-1. These curves show the MTF of a perfect lens as a function of focal position displacement from best focus, $k\delta_0$ (δ_0 corresponds to 1/8 wavelength of optical path difference).

The first thing to note about the curves is that the value of the MTF at zero frequency always remains unity with focus variation. This value of the MTF at n = 0 multiplies the zero frequency (dc) term of the scene spectrum, I(0, 0) which corresponds to the total radiant power in the image.

$$I(0, 0) = \int_{-\infty}^{+\infty} \int_{-\infty}^{+\infty} i(x, y)\, dx\, dy$$

The second thing to note is the sensitivity to defocus of different spatial frequencies from dc to the lens cutoff frequency. We are interested in the defocus change of contrast transmission for a particular frequency region relative to the best focus condition. To emphasize this change, the curves of Fig. 1-1 are replotted normalized to the best focus MTF. These new curves are shown in Fig. 1-2, where the ordinate values of a curve corresponding to a defocus position, k, are $(MTF)_k/(MTF)_0$. This new plot shows that at the extreme values of zero frequency and the lens cutoff frequency, n_c, the sensitivity to defocus is 0, while at approximately $0.5n_c$, the sensitivity is maximum. It should be remembered that the actual sensitivity of the image to defocus is the MTF curve weighted by the scene frequency content, i.e., $I(n_x, n_y) = O(n_x, n_y)\, \tau(n_x, n_y)$. Note that discrepancies about $1.0n_c$ are due to computer error.

1.1.4 Deriving a Measure of Best Focus From Image

In the previous section, the spatial frequency domain representation was used as an aid in characterizing the image as a function of defocus. The motivation for using this representation is similar to that for using the electrical frequency representation for investigating amplifier response; the frequency domain approach often gives more insight into the prediction of the response of a linear system, as well as providing a simpler mathematical form. This certainly has been the case here, where the difficulty of performing a convolution in the space domain has been replaced by a simpler multiplication in the frequency domain.

The insight gained by means of the frequency domain approach leads to the conclusion that best focus can be sensed by a maximization of the volume under the surface formed by $|I(n_x, n_y)|^2$. It can be shown by an application of Parseval's theorem that this is equivalent to a maximization of the volume formed by the surface $|i(x, y)|^2$. The proof of this two-dimensional problem will be outlined below for the one-dimensional case to simplify the mathematical form. An area, rather than a volume, is maximized here, but the extension from one to two dimensions only requires writing the corresponding two-dimensional integral for all the one-dimensional integrals presented below.

For this derivation we assume a scene, o(x), its image i(x), and their corresponding spatial frequency Fourier transforms, O(n) and I(n).

$$I(n) = \int_{-\infty}^{+\infty} i(x) \exp(-j2\pi nx)\, dx$$

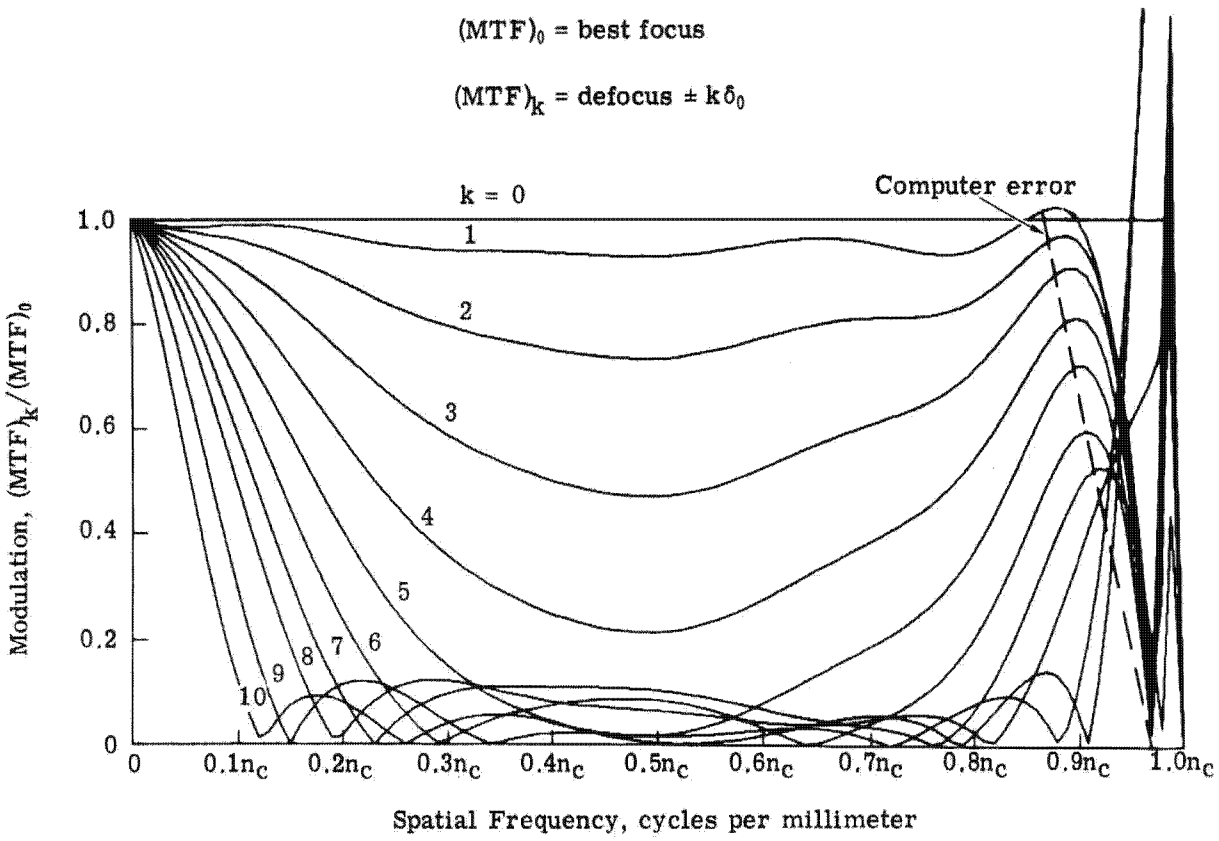

Fig. 1-2 — Normalized plot of MTF of perfect lens versus defocusing, $\pm k\delta_0$

The lens is characterized by $\tau_0(n)$ for best focus and $\tau_k(n)$ for various defocus conditions, k. The image is now characterized by $I(n) = O(n)\tau(n)$. In addition, we consider the Wiener spectrum of the image, which is defined as

$$G(n) = I(n)I^*(n) = |I(n)|^2$$

A new quantity, V, is defined

$$V = \int_{-\infty}^{+\infty} G(n)\, dn = \int_{-\infty}^{+\infty} |I(n)|^2\, dn$$

Solving first for the Wiener spectrum, G(n), we obtain

$$G(n) = |I(n)|^2 = |O(n)\tau(n)|^2 = |O(n)|^2 |\tau(n)|^2$$

Substituting into the integral for V_k, and noting that $(MTF)_k = |\tau_k(n)|$, we have

$$V_k = \int_{-\infty}^{+\infty} |O(n)|^2 |\tau(n)|^2\, dn$$

Since $|\tau_0(n)| \geq |\tau_k(n)|$ for all frequencies, n, the integral is always maximized for $|\tau_0(n)|$, the best focus MTF. It also follows that $V_0 \geq V_k$.

We are now faced with the maximization of an integral of a frequency domain function in order to sense best focus. From an extension of the convolution integral theorem, however, a useful relationship can be derived

$$\int_{-\infty}^{+\infty} i_1(x)i_2(x) \exp(-j2\pi mx)\, dx = \int_{-\infty}^{+\infty} I_1(m - n)\, I_2(n)\, dn$$

For the case $m = 0$, we develop Parseval's theorem for the product of two functions

$$\int_{-\infty}^{+\infty} i_1(x)i_2(x)\, dx = \int_{-\infty}^{+\infty} I_1(-n)I_2(n)\, dn$$

If $i_1(x)$ is a purely real function, then

$$I_1(-n) = I_1^*(n)$$

and

$$\int_{-\infty}^{+\infty} i_1(x)i_2(x)\, dx = \int_{-\infty}^{+\infty} I_1^*(n)I_2(n)\, dn$$

For the case $i_2(x) = i_1(x)$

$$I_2(n) = I_1(n)$$

Therefore

$$\int_{-\infty}^{+\infty} [i_1(x)]^2 \, dx = \int_{-\infty}^{+\infty} |I_1(n)|^2 \, dn = V$$

Extending the relationship for V to two dimensions, we have

$$V = \int_{-\infty}^{+\infty} \int_{-\infty}^{+\infty} [i(x, y)]^2 \, dx \, dy$$

$$= \int_{-\infty}^{+\infty} \int_{-\infty}^{+\infty} |I(n_x, n_y)|^2 \, dn_x \, dn_y$$

It can be concluded that the process of squaring the image intensity function, i(x, y), and integrating over the extent of the finite image will yield a value of V which is maximized for best focus.

A more general integral of the function $[i(x, y)]^r$ over the extent of the finite image might be considered. It has been shown above that with a variation in focal position, the case $r = 2$ provides for a maximization of the value of the integral for best focus. For the case $r = 1$, there is not change in the value of the integral, since this is just the total radiant power in the image. Therefore, although it cannot yet be shown rigorously, it would appear that for other values of r, namely $1 \leq r \leq 2$, a maximization of the values of the integral would also be achieved at best focus. It could also be concluded that values of the integral would show an increasingly sharper maximum as r increases above 1; this is shown diagrammatrically in Fig. 1-3. The curves are normalized to the maximum value of the integral. In addition, the case $r > 2$ should also produce a maximum, and the case $0 \leq r \leq 1$ should produce a minimum at best focus.

The previous paragraphs show that the overall change in the image with focus variation can be characterized by the Wiener spectrum of the image, and, in particular, that certain portions of the spatial frequency content of the image are more sensitive than others. Therefore, the merits of any focus sensing mechanism are relative to its ability to measure frequency content.

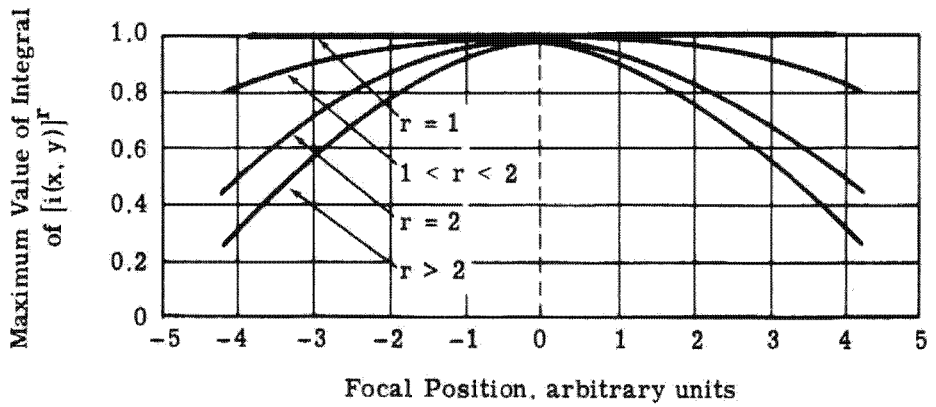

Fig. 1-3 — Schematic representation of maximization of the integral of $[i(x, y)]^r$

2. RECENT TEST RESULTS AND CONCLUSIONS

In order to substantiate the analysis shown in Section 1, data was taken on the vidicon focus sensor which shows the relative video power amplitude change with focus for two particular scenes.

It is important to stress that, although Fig. 1-2 indicates that the maximum sensitivity to defocus occurs at 0.5 of the lens cutoff frequency, the actual sensitivity of the image to defocus is the MTF curve weighted by the scene frequency content.

Figs. 2-1 and 2-2 show the change in relative video power with a change in focus over a 0.020-inch change in focus position. The frequency spectrum is detectable to 5 megahertz for the random scene (Fig. 2-1), and to 4 megahertz for the airport scene (Fig. 2-2).

In addition, a static focus curve was plotted using the random scene (Fig. 2-3). Video detector output was plotted against position out to 0.060 inch from position of best focus. For this scene, a sensitive range of ±0.030 inch was evident. However, it is felt that the linear range can be extended out to possibly 0.100 inch under real scene conditions with appropriate post-filtering techniques. One possibility would be to utilize two modes, i.e., fine and course. Relatively wide band postdetection filtering would provide a wide linear range for acquisition. A high sensitivity mode could then be utilized for final focusing. This mode would use postdetection filters which would eliminate more of the insensitive, low spatial frequencies.

Preliminary data was taken on the effects of astigmatism on focus sensitivity. Using a bar chart for scene content, and an eighth and quarter diopter cylindrical lens of positive power, the cylindrical lens was oriented in one position in the cone between the vidicon and the f/4.8 lens. Then the bar chart was repositioned with bars running vertical, horizontal, and at 45 degrees. Each time the position of best focus was obtained. This data is shown in Table 2-1.

Table 2-1 — Change of Focus with Astigmatism Introduced

	Position of Bar Chart		
Diopter	Vertical	45-Degree	Horizontal
0.125	+0.012	0	-0.016
0.250	+0.016	0	-0.015

Note: + indicates increase in focal length.

Further testing will be conducted with real scene inputs while introducing rotation of the cylindrical lens.

Further data can and will be taken on the breadboard unit relative to the problems discussed.

An important advantage of using the vidicon for focus sensing is the ability to see what information is being used to provide best focus. If a display is available, the correlation involved provides a degree of assurance not available from sensors of the scanning reticle variety.

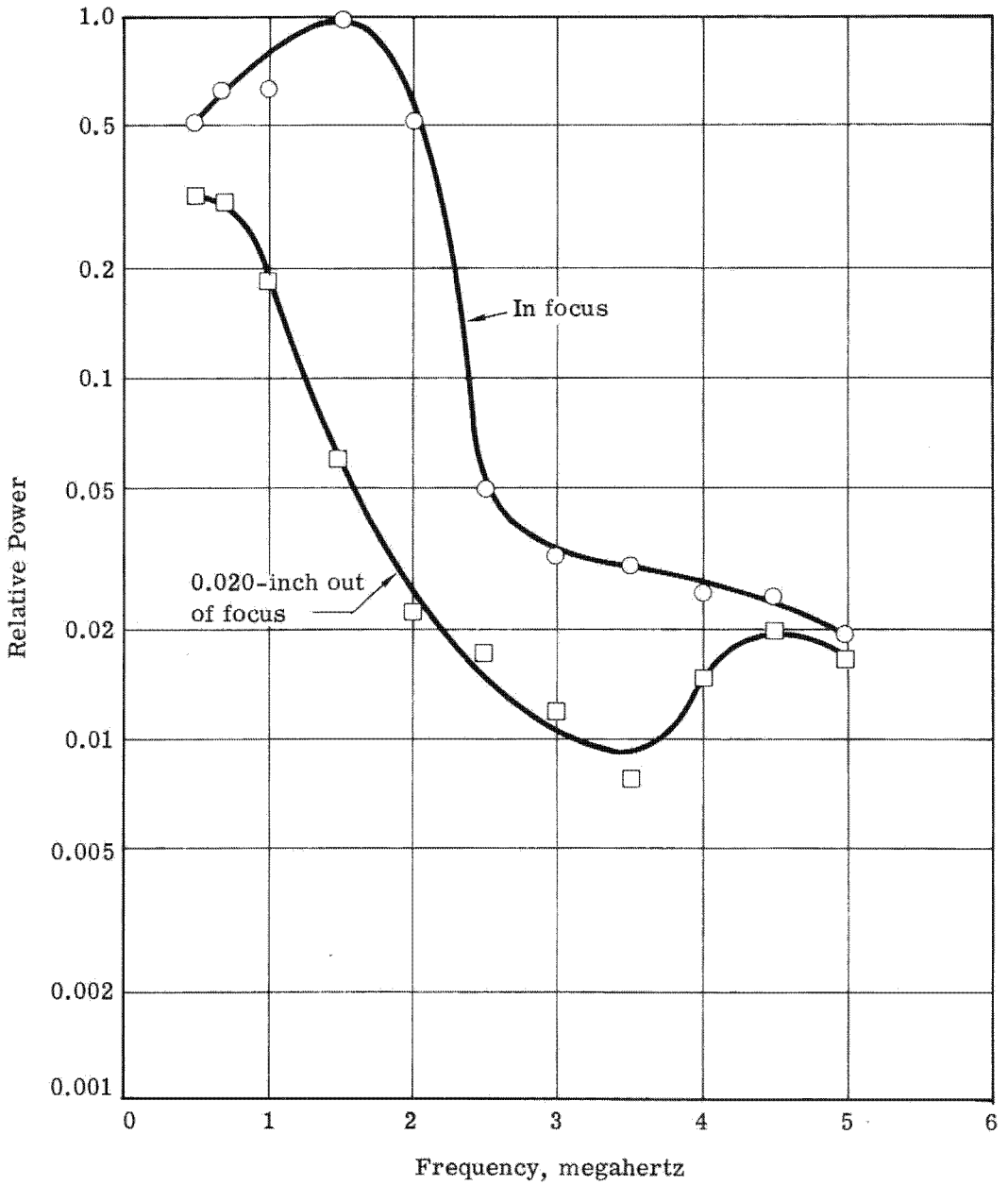

Fig. 2-1 — Power spectrum: illumination = 0.68 foot-candle, random scene, high contrast, f/4.8 lens

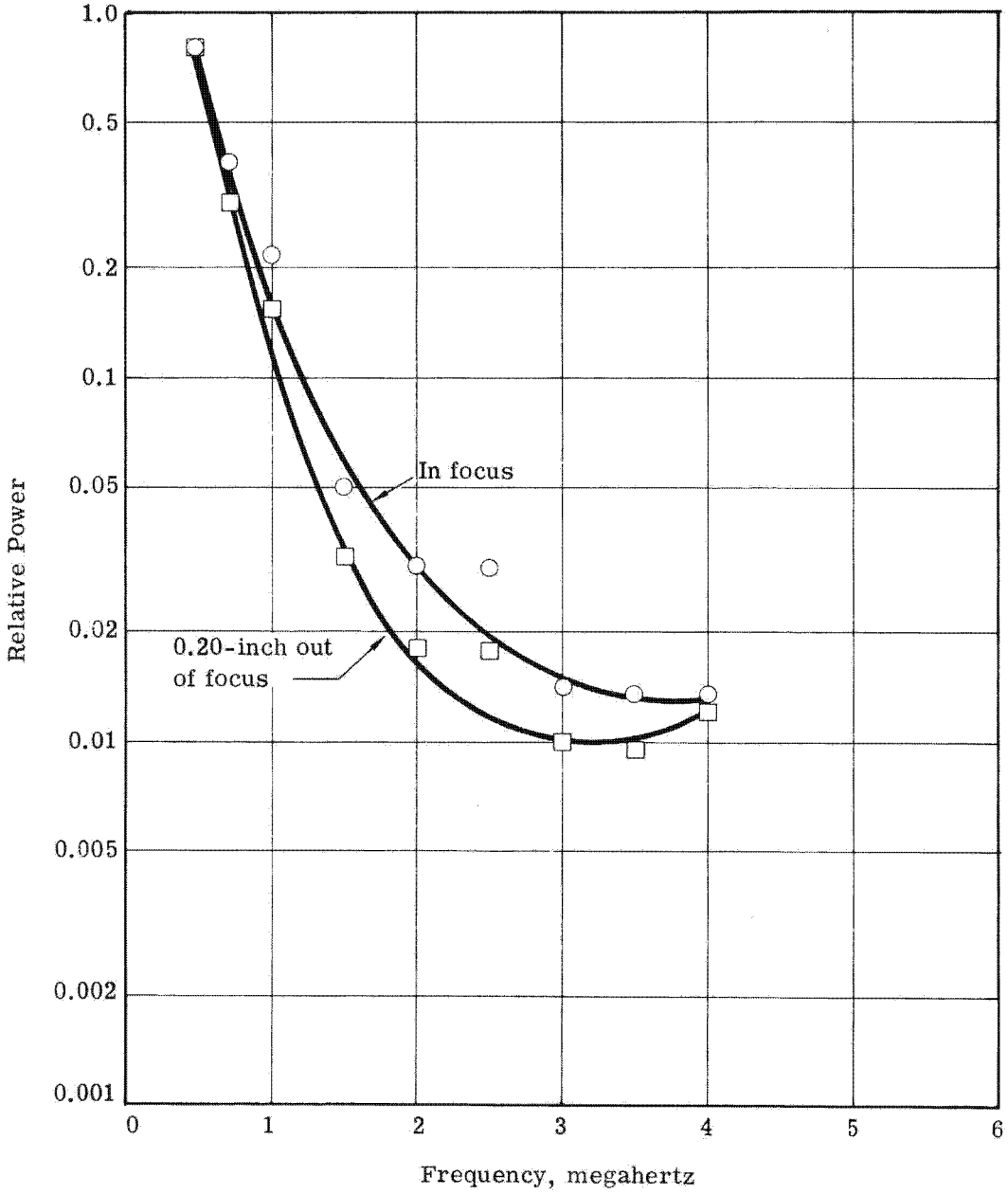

Fig. 2-2 — Power spectrum: illumination = 0.56 foot-candle, airport scene, medium contrast, f/4.8 lens

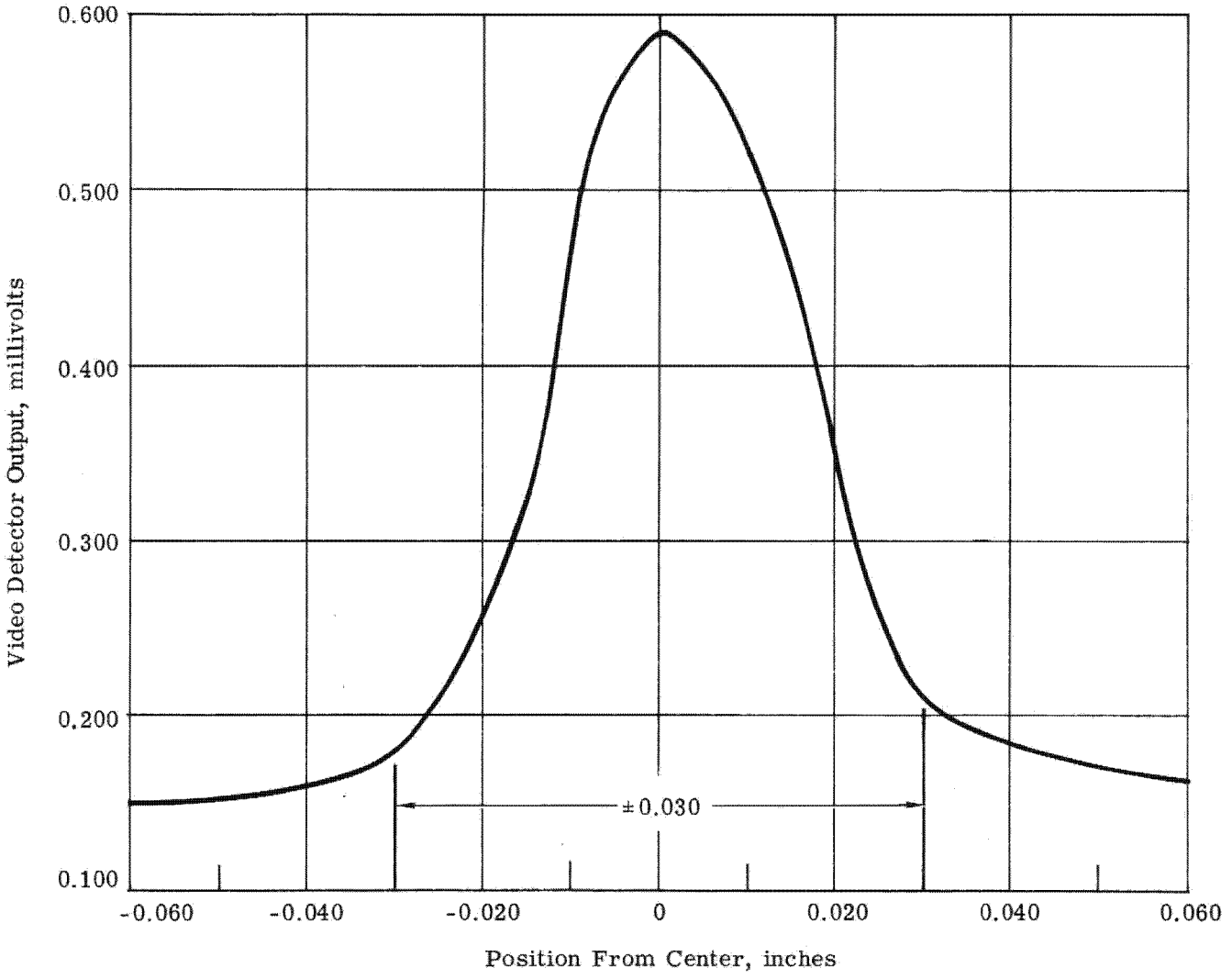

Fig. 2-3 — Pseudo-random scene: brightness (measured) = 90 foot-lamberts, 1.0 megahertz high-pass filter, f/4.8 lens

3. REAL SCENE FOCUS SENSOR FINAL REPORT

3.1 CONCLUSIONS AND RECOMMENDATIONS

A vidicon focus sensor has been designed and a breadboard model has been constructed. The precision of its response is proportional to the data integration rate or response time. For an integrator time constant of about 2 seconds, focus resolution of less than 10^{-4} inch has been obtained using an f/5 lens and a real scene test target of moderate contrast with about 200 foot-lamberts brightness. Details of test results obtained are discussed in following sections. The sensor developed exhibits low drift and good sensitivity. However, we suggest that further test evaluation of the equipment be made to augment the results obtained in the relatively limited time available since construction of the complete sensor.

The test apparatus was designed to allow considerable flexibility in the test modes available. Modulation amplitude, frequency, and waveform, loop parameters, and target characteristics are all variable to allow evaluation over a wide range of operating conditions. In addition, the camera carriage is easily adapted to other cameras or detectors.

A separate study of alternate detectors was conducted. This study primarily examined the suitability of image dissector tubes compared with vidicon tubes. The primary advantage of the dissector tube appears to be that it is not a storage detector, as is the vidicon, and image size modulation resulting from focus modulation does not result in image smear. The study shows a favorable evaluation of dissector sensitivity. Experimental studies of a high resolution dissector camera should be conducted with the same test apparatus to compare image dissector with vidicon focus detection capability.

3.2 INTRODUCTION

At the inception of the vidicon focus sensor development program, it was realized both from theory and from experimental side results of other camera investigations that the power contained in the high frequency portion of the video spectrum is modulated by deviation of the detector from the position of best focus. The IR&D program for development of the vidicon camera as a detector for motion (V/h) sensing had shown the usefulness of the vidicon detection and the video signal processing for separating portions of the image power spectrum to obtain a measure of image quality. Initially, the prime objective of this program was to obtain a measure of the capability of the vidicon camera for detection of its target plane from the position of best focus. A high quality vidicon camera was to have been acquired and data showing variation in selected portions of the high frequency video power spectrum with variations in focal distance were to have been obtained. However, the initial "focus curves" obtained with a high quality camera were so encouraging that it was decided to proceed with the breadboard design and construction of a complete sensor. This task was scheduled for completion during the reporting period.

The major problem encountered in obtaining the results desired was not a technical barrier but merely the scope of work, that is, the completion of a full sensor within the limited time period available. However, a breadboard was completed and preliminary results were obtained. The following discussion outlines the design of the full vidicon focus sensor and experimental results from its evaluation. The "Description of Work" is a general description of tasks completed, including the procurement, design, and evaluation. The technical discussion sets forth important design parameters and test results. The discussion also describes theoretical considerations for the use of other image detectors in the same sensor configuration.

3.3 DESCRIPTION OF WORK

3.3.1 Test Design and Setup (Reference Figs. 3-1 and 3-2)

The test setup was designed to provide maximum flexibility of system parameters during test. The test setup is illustrated in Fig. 3-1.

The table on the left holds a variable intensity light source. The remainder of the optical setup is mounted on an optical rail, 10 feet long by 8 inches wide.

The translucent screen and the Zeiss f/180-millimeter lens are each held to the rail by quick disconnect clamps.

The vidicon camera is mounted behind the lens on a three-carriage mechanism which is also quick clamped to the optical rail.

The first carriage is the modulation carriage which provides for motion between the camera and the transverse carriage along the optical path. The modulation carriage is servo driven through a lead screw. Modulation is applied in the form of a signal from a standard laboratory oscillator, causing the carriage to translate along the optical path with simple harmonic motion.

The second carriage provides for motion across the optical path and is manually set with a micrometer.

The third carriage is the position carriage which provides for motion along the optical path between the optical rail and the first two carriages. The position carriage is servo driven through a gear train and lead screw. The servo loop is closed through the vidicon camera and signal processing circuitry to position the carriage at the true focus position.

The two servoamplifiers for the modulation and position loops are also mounted on the optical rail.

A second table and a 6-foot, 6-inch rack contain the remaining electronics: video processing circuits, camera control circuits, and auxiliary equipment such as power supplies, spectrum analyzer, digital voltmeter, video monitor, and modulation oscillator.

3.3.2 Component Design and Evaluation

3.3.2.1 Sensor Mechanism

The mechanical aspect of the automatic focus sensor servo system consists mainly of two parts: the focus modulation and the carriage drive. However, both subassemblies have been designed around the same basic principle. The principle is the use of a fine pitch lead screw to

SPECIAL HANDLING
SECRET

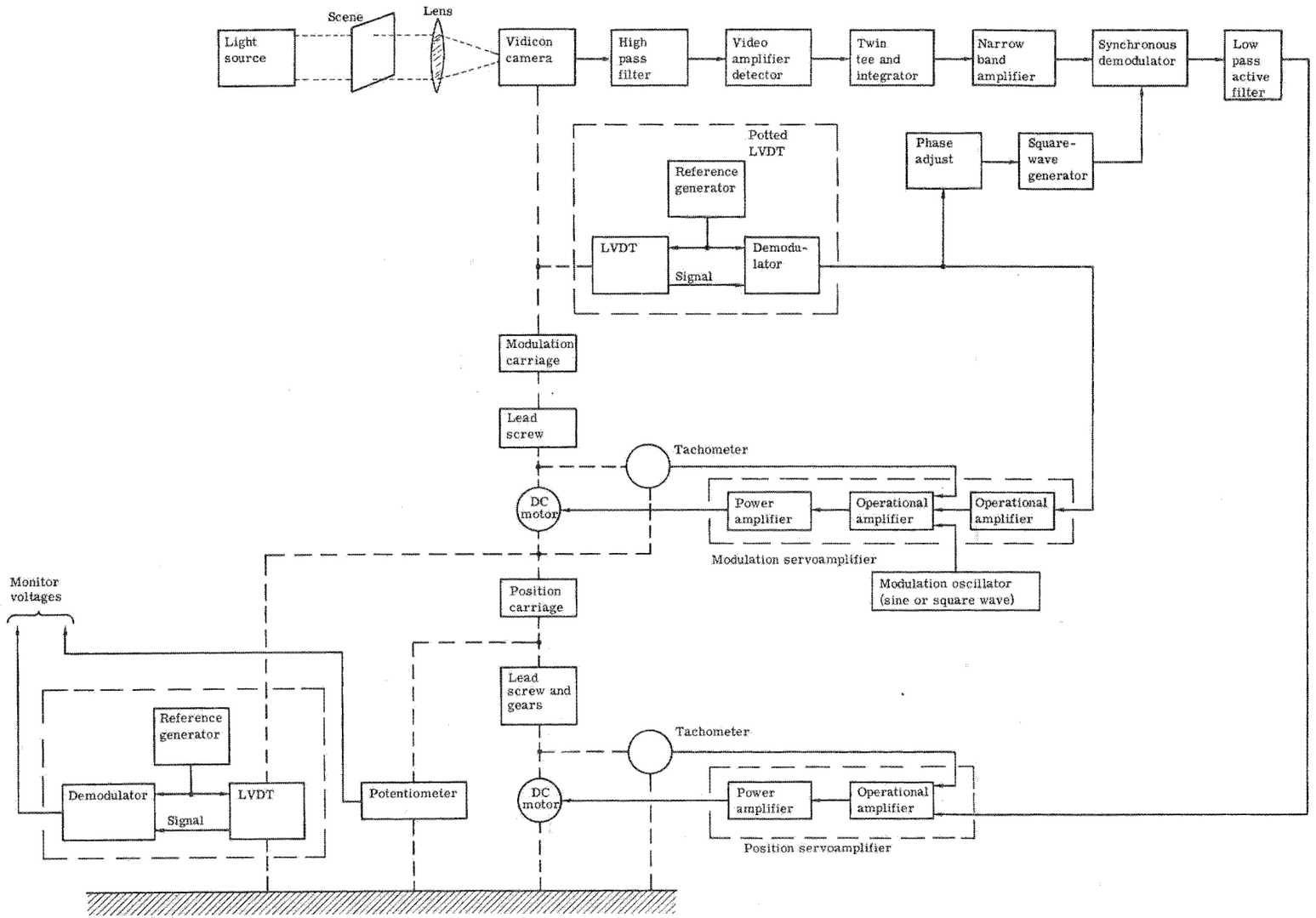

Fig. 3-1 — Real scene focus sensor block diagram

SECRET

SECRET

Approved for Release: 2021/12/09 C05137011

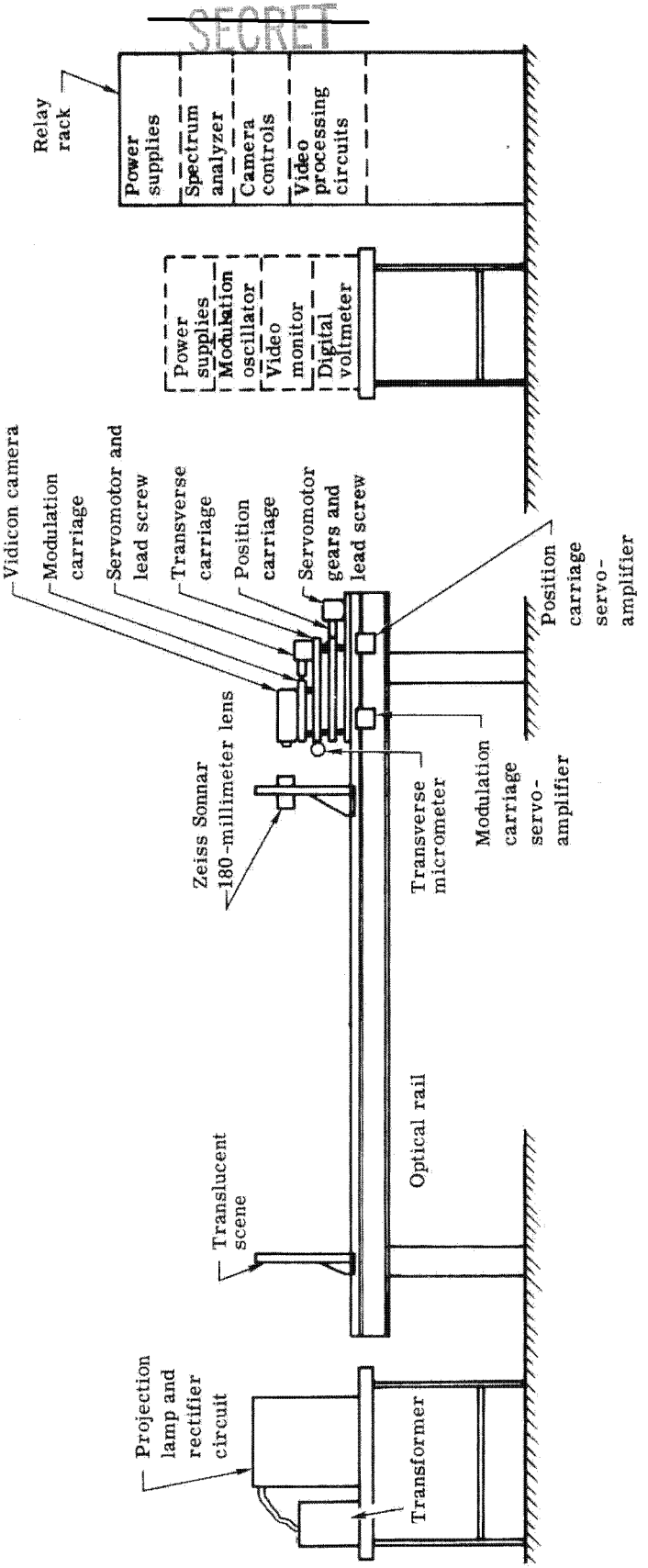

Fig. 3-2 — Real scene focus sensor test setup

provide accurate linear positioning. The lead screw used in both cases is a 1/2-inch diameter, 40-pitch lead screw with each rotation of the screw corresponding to 0.025 inch of travel.

The main difference between the assemblies is that while both units are driven by approximately 25-inch-ounce torque motors, the carriage drive lead screw is at a 1:5 speed ratio to the motor, whereas the focus modulator is directly driven at a 1:1 ratio.

Both assemblies contain an inertia disc to smooth out perturbations, and both assemblies contain LVDT linear position indicators.

The comparatively friction-free motion that must accompany a device of this type is accomplished by mounting two spring-loaded micrometric stages in tandem: one for the focus modulator, and one for the carriage drive.

3.3.2.2 Camera/Lens System

Lens

The lens is a Carl Zeiss NR. 2613428, Sonnar 1:4.8, 180-millimeter focal length.

Camera

The camera is a Granger Association Model V-1000 vidicon camera having a horizontal resolution of 1,000 TV lines per picture width. The camera and associated synchronization rack are all solid state (except for the vidicon tube itself). The resolution specification mentioned above in terms of TV standards is translated to optical and electronic terms as follows:

Resolution at vidicon face: 25 lines per millimeter
Frequency response: -3 decibels at 16 Mhz (525-line raster)
S/N ratio: 20 decibels at 0.5-foot-candle illumination

3.3.2.3 Video Processing Electronics

The following components constitute the video system: video amplifier, envelope detector, video integrator, narrow band amplifier, synchronous detector, and modulation integrator.

Video Amplifier

The video amplifier contains a high pass filter and a video amplifier with response from 0.5 to 50 Mhz, with a 40-decibel gain.

Envelope Detector

The envelope detector is a peak-to-peak average power detector functioning in its linear region with a power loss of 6 decibels.

Video Integrator

The integrator is an RC circuit with a time constant of 100 milliseconds. It was empirically determined that no significant improvement was gained by higher time constants.

Narrow Band Amplifier

The narrow band amplifier provides a 40-decibel gain from 0.1 to 10 hertz; phase is constant within 5 degrees in this band.

Synchronous Detector

The synchronous detector is a full-wave demodulator using two FET gates driven out of phase and a differential amplifier; the gate drive is a square wave derived from the modulation carriage position transducer (LVDT).

Modulation Integrator

A variable integrator is provided at this point for servo loop optimization. Since provision is made for 0.1- to 10-hertz modulation, 1- to 10-second integration is provided.

3.3.2.4 Modulation Servo

The focus modulator configuration is outlined in the overall sensor description. Modulation is accomplished by moving the detector portion of the vidicon camera (i.e., the vidicon and its control magnetic components which are attached by cable with the camera electronics) back and forth along the lens optical axis in a controlled fashion so that the modulation excursion is centered about the point of best focus.

Fig. 3-3 is a functional block diagram of the modulation servo. The overall configuration is that of a position servo designed to give modulation precision consistent with the focus accuracy desired. The servoamplifier is a combined, integrated, and discrete component solid-state design that drives the modulator lead screw through a directly coupled dc servomotor. An inertia wheel on the lead screw shaft provides mechanical filtering against mechanical disturbances that result from frictional loading variation on the lead screw. In addition, a tachometer directly coupled to the lead screw provides feedback to linearize and stabilize the apparent servoamplifier-motor characteristic. A linear variable differential transformer (LVDT) with self-contained excitation oscillator and demodulator provides precision sensing of the modulation carriage with respect to the main carriage. This device, together with the command oscillator, provides the primary modulation control. The command oscillator is a commercial (Hewlett-Packard Model 212A) unit that can provide variable amplitude and frequency modulation of low distortion and high stability command to the modulation servo. Normally, the modulation command is sinusoidal. In addition, a selector switch allows selection of triangular or square-wave motion. Sinusoidal modulation was used in the tests performed. However, square-wave modulation holds interest for future evaluation because of its capability for minimizing smear due to image retention. The modulator servo provides excellent sinusoidal modulation in the frequency range of 0.1 to 10 hertz.

3.3.2.5 Closed Loop Sensor

The overall block diagram (Fig. 3-1) is essentially a diagram of the closed loop focus sensor. This shows the interrelationships of the camera to the modulator, the positioning mechanisms, and the video electronics. As described previously, the modulator carriage motion modulates the high frequency portion of the video spectrum, producing a fundamental signal of the same frequency as the modulation if the position of best focus is not at the center of the modulation motion. After video detection, the synchronous demodulator switches this signal synchronously with the modulator carriage crossing of the center position (zero crossing) to provide rectification of the fundamental signal. Since the fundamental focus-indication frequency is in phase (and not at quadrature) with the modulation signal, the modulator output includes a component proportional to the focus error. The output of the demodulator is filtered by the low-pass filter which smooths and alternates the ac noise (without attenuating the signal) within the limits of the filter operation

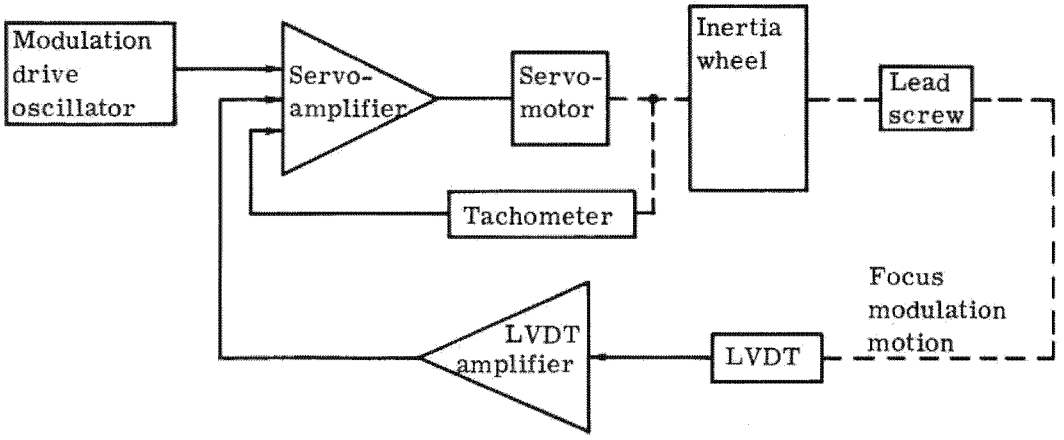

Fig. 3-3 — Modulator functional block diagram

on the signal and noise spectra. The synchronous modulation and demodulation, together with the filtering, essentially rejects any apparent signal that is uncorrelated with the modulation process. This minimizes the effects of sensor gain variations and noise processes from nearly all sources. In addition, second harmonic components associated with the detection process but not containing useful position data are rejected. A large portion of the tests to be performed involve optimization of the loop gain and filter time constant.

A servoamplifier, servomotor, and tachometer feedback nearly identical to that used for the modulator drive is used for driving the main carriage. However, a 5:1 gear ratio is used between the motor and lead screw, providing better isolation from the larger carriage lead. The tachometer loop provides good integration of the filter output as well as stabilization of the motor-drive characteristic.

A monitoring potentiometer is provided between the lead screw shaft and bedplate, and an LVDT indicates position of the carriage with respect to the bedplate.

3.3.3 Tests

3.3.3.1 Focus Detector Test Procedure (Static Measurements)

The following parameters were varied for the purpose of empirical establishment of optimum compromise points:

1. Video detector (square law versus linear)
2. Video postdetection integration time
3. Video predetection high pass filter

Other parameters carried as variables for a series of measurements were:

1. Light level (0.1, 0.5, 1.0 foot-candle at vidicon)
2. Scene
3. Contrast (by means of changing scenes)

The procedure used is described below.

Series I

A random art-type (no. 4082) scene with an illumination of 0.5 foot-candle impinging on the vidicon face was used. The procedure is as follows:

1. Detector selection: with all other parameters constant, select one detector operating level; leave constant for the remainder of the program.

2. Comparison test: for purposes of comparison with other focus sensing schemes, obtain output versus linear position change using an integration time of 1.0 second and a video predetector filter of 0.5-Mhz cutoff.

3. Integration time selection: with the predetection filter at 0.5-Mhz cutoff, obtain focus detection and rms fluctuation data for: τ = 0.001, 0.005, 0.01, 0.05, and 0.1 second. Select a value for optimum operation.

4. High-pass filter selection: obtain focus detection and rms fluctuation data at τ = 0.01 second for three predetection filters: roll off at 0.5, 1.0, and 5.0 Mhz. If any filter produces a significantly degraded result, eliminate it from all succeeding tests.

Series I should be represented by the following data:

1. Comparison test, f = 0.5 Mhz, τ = 1.0 second
2. Integration time selection, f = 0.5 Mhz, and τ = 0.01 second
3. High-pass filter selection, f = 1.0 Mhz, and τ = 0.01 second

Series II—Illumination and Contrast

A random art type scene was again used. Illumination and scene contrast were varied. The values f = 1.0 Mhz, and τ = 0.01 second, are as determined above.

1. Illumination = 0.1 foot-candle at vidicon
2. Illumination = 1.0 foot-candle at vidicon
3. Scene changed to 2:1 contrast; 0.1 foot-candle
4. Scene changed to 2:1 contrast; 0.5 foot-candle
5. Scene changed to 2:1 contrast; 1.0 foot-candle

Series III—Real Scene

All tests of Series II were run using a real scene instead of the random art-type scene.

3.3.3.2 Focus Sensing Test Procedure (Modulation Measurements)

Post- and predetection filtering will remain constant for all tests, at predetermined optimum compromise points.

Modulation Frequency Selection

A real scene with an illumination of 0.5 foot-candle at vidicon was used.

Obtain data at 0.1, 0.3, 1, and 10 hertz to analyze the effect of vidicon scene retention; select highest usable modulation frequency for further series. Using above electrical parameters, vary scene, illumination, and contrast; obtain input volts versus position data.

3.3.4 Alternate Detector Study (Analysis of Vidicons and Image Dissectors)

Table 3-1 gives the performance and physical characteristics of image dissector and vidicon tubes by a number of manufacturers. The tube that is presently being used in the automatic focus control system (AFCS) is a GEC, no. 8507, vidicon. The performance of this tube is comparable to the GE, no. 8507, and the RCA, no. 8507, vidicon tubes, which are listed in Table 3-1.

The luminous sensitivity and dark current noise was found to be nearly the same for the image dissectors with S-20 response and the vidicon used in the AFCS when reference was made to the same electrical bandwidth, $\Delta\nu$. In addition, the resolution of the image dissector tube was found to be nearly the same as that of the vidicon tube of comparable size. Therefore, one would expect equivalent performance under the same conditions of illumination. From the standpoint of the present application, the most significant difference between the vidicon and dissector tubes is found in the light integration time and in the amount of video signal holdover, which for a given frame is represented as a decimal fraction of the magnitude of the video signal in the preceding frame.

The light integration time in all instances was based on an electrical bandwidth of 5 megacycles and on complete utilization of the photosensitive surface in each of the tubes. For the vidicon tube, the integration time is equal to the frame time and is determined by the number of resolution elements in the frame divided by the electrical bandwidth. The frame time for all of the vidicons was long by comparison with the standard video frame time by virtue of their high resolution. Since, on the other hand, the photosensitive surface in the image dissector tube is photoemissive rather than photoconductive, as in the case of the vidicon, it cannot integrate or store electrons. The integration time for the dissector tube is thus determined by the dwell time of the electronic image at the anode aperture plate as determined by the sampling, or sweep, rate and by the dimensions of the anode aperture. The integration time of the image dissector tube is $\Delta\nu^{-1} = 2 \times 10^{-7}$ second.

There is no video signal holdover in the image dissector tube since the intensity of the electron beam through the anode aperture is entirely determined, if one discounts dark current, by the number of photons reaching the conjugate point on the photocathode at that instant. On the other hand, stored charge is not completely erased during readout of the photoconductive surface in the vidicon. This results in video signal holdover which will be read out as spurious images in successive frames. The magnitude of this signal under moderate illumination is about 0.03, or 3 percent, for most vidicons.

A recently developed vidicon tube that employs a Pb0 target, which is known as a plumbicon, apparently has greatly reduced image retention as its principal advantage. Information on this tube could not be obtained in time for inclusion in this report.

Another relatively recent development is a vidicon employing a secondary electron conduction (SEC) target. The primary advantages of the SEC target is in its high signal current gain and in its ability to integrate electrons over long periods of time, which makes it adaptable to low light level imaging. Table 3-1 indicates that the Westinghouse SEC vidicon, no. WX-30152, has a very high luminous sensitivity as its only significant advantage over conventional vidicons.

The performance of the AFCS is based on changes in the high frequency portion of the power frequency spectrum, P_{hf}, of the video signal from the image tube employed in the system as the image on the photosensitive surface is alternately focused and defocused. The changes in P_{hf} can, of course, be explained by the changes in the transfer function of the objective lens in the

focused and defocused states. However, when one considers the lens and image tube combination, it becomes evident that the performance characteristics of the tube have a significant affect, also, on the power frequency spectrum for the system and on the magnitude of changes in P_{hf} for a given focal shift. The total affect of the image tube on the performance and sensitivity of the AFCS can be expressed by a merit figure, m, which is calculated for one set of system and lens objective characteristics. In the expression for the term m given below, optimum performance and sensitivity is achieved when the value of m is a minimum.

In establishing a merit figure for each image tube in Table 3-1, it is assumed that the scene brightness in each case is sufficient to meet the following condition:

$$C^2 K n_t t > R_T^2 A$$

where K = quantum efficiency
n_t = photon rate on photosensitive surface
t = integration time
R_T = resolution of tube (lines/inch)
A = area of useful portion of the photocathode surface
C = contrast sensitivity

Then, if we further assume that $\Delta\nu = 5 \times 10^6$, then m may be defined as follows:

$$m = \frac{\left[2 \times 10^{-7} \left(\frac{R_T}{R_L}\right)^2 + t\right]^{1/2} f}{(R_T^2 + R_L^2)^{1/2} (1 - \nu)}$$

where f = frequency of defocusing motion
R_T = resolution of tube (lines/inch)
R_L = resolution of lens (lines/inch)
t = integration time
ν = video signal holdover

For the case where R_L = 1,000 lines/inch and f = 1 cps, then:

$$m = \frac{(2 \times 10^{-13} R_T^2 + t)^{1/2} f}{(R_T^2 + 10^6)^{1/2} (1 - \nu)}$$

It may be noted that the merit figure will have no significance when tf > 1/2, since the image tube will then integrate out any changes in the modulation transfer function. As a result, $\Delta P_{hf} = 0$.

The lower merit figures for the image dissector tubes indicates that they will provide greater sensitivity and more accurate focus control than the vidicon tube. In addition, the luminous sensitivity and dark current noise of the S-20 image dissector should make them photometrically comparable to the vidicon. By virtue of their comparable size to the presently employed GEC 8507, either the ITT F4011, or ITT F4012, are recommended as superior replacement tubes.

SPECIAL HANDLING
~~SECRET~~

Table 3-1 — Performance of Vidicons and Image Dissectors

Manufacturer	Tube No.	Type	Spectral Response	Minimum Luminous Sensitivity, microamps/lumen	Dark Current Noise, microamps (5 mc bandwidth)	Resolution lines/inch	Weight	Maximum Diameter, inches	Overall Length, inches	Focusing/ Deflection	Typical ENI, lumens	Vidio Signal Holdover	Light Integration Time, seconds (5 mc bandwidth)	Merit Figure
ITT	F4011	Dissector	S-20	100	0.02	1,700	5.5 oz	1.5	8.2	M/M	10^{-13}	0	2×10^{-7}	$2.3 \times 10^{-}$
ITT	F4012	Dissector	S-20	100	0.02	1,700	2.6 oz	1.0	6.75	M/M	10^{-13}	0	2×10^{-7}	$2.3 \times 10^{-}$
Westinghouse	WL-23111	Dissector	S-20	180	0.04	3,000	24 oz	3.0	20.0	M/M	10^{-13}	0	2×10^{-7}	$4.8 \times 10^{-}$
CBS	CL-1201	Dissector	S-11	50	0.01	3,000		3.5	12	M/M	10^{-13}	0	2×10^{-7}	$4.8 \times 10^{-}$
CBS	CL-1147	Dissector	S-11	30	0.02	1,000	180 gm	1.5	6.25	E/E	10^{-13}	0	2×10^{-7}	$4.6 \times 10^{-}$
ITT	FW-146	Dissector	S-1	12	2	3,000		4.5	14	M/M	3×10^{-11}	0	2×10^{-7}	$4.8 \times 10^{-}$
ITT	FW-118	Dissector	S-1	20	3			2	6.3		10^{-10}	0	2×10^{-7}	
GE	8507	Vidicon	S-18	150	0.02	2,000		1.125	6.25	M/M		0.03	0.2	$2.1 \times 10^{-}$
GE	8541	Vidicon	5500 A (peak)	150	0.02	2,000	2.0 oz	1.125	6.25	M/M		0.03	0.2	$2.1 \times 10^{-}$
Machlett	2058G	Vidicon	S-18	1	0.08	2,000	10.0 oz	2.25	12.0	M/M		0.03	1.0	$4.8 \times 10^{-}$
RCA	8521	Vidicon	5500 A (peak)	35	0.02	1,000		1.6	8.0	M/M		0.03	0.2	$3.3 \times 10^{-}$
Westinghouse	WX-30152	SEC vid.	S-20	9,000		1,000		2.75	12.4	E/M		0.03	0.3	$4.0 \times 10^{-}$
RCA	8480	Vidicon		4		1,400		1.6	10.375	E/M		0.03	0.3	$3.2 \times 10^{-}$
GEC	TD 8484	Vidicon	4800 A (peak)	200	0.02	1,700		1.125	6.250	M/M		0.03	0.2	$2.4 \times 10^{-}$
RCA	8507	Vidicon	5500 A (peak)	150	0.02	2,000	2.0 oz	1.125	6.250	M/M		0.03	0.2	$2.1 \times 10^{-}$

Approved for Release: 2021/12/09 C05137011

~~SECRET~~
SPECIAL HANDLING

~~SECRET~~
SPECIAL HANDLING

SPECIAL HANDLING
SECRET

Table 3-1 — Performance of Vidicons and Image Dissectors

Manufacturer	Tube No.	Type	Spectral Response	Minimum Luminous Sensitivity, microamps/lumen	Dark Current Noise, microamps (5 mc bandwidth)	Resolution lines/inch	Weight	Maximum Diameter, inches	Overall Length, inches	Focusing/ Deflection	Typical ENI, lumens	Vidio Signal Holdover	Light Integration Time, seconds (5 mc bandwidth)	Merit Figure
TT	F4011	Dissector	S-20	100	0.02	1,700	5.5 oz	1.5	8.2	M/M	10^{-13}	0	2×10^{-7}	2.3×10^{-6}
TT	F4012	Dissector	S-20	100	0.02	1,700	2.6 oz	1.0	6.75	M/M	10^{-13}	0	2×10^{-7}	2.3×10^{-6}
Vestinghouse	WL-23111	Dissector	S-20	180	0.04	3,000	24 oz	3.0	20.0	M/M	10^{-13}	0	2×10^{-7}	4.8×10^{-6}
BS	CL-1201	Dissector	S-11	50	0.01	3,000		3.5	12	M/M	10^{-13}	0	2×10^{-7}	4.8×10^{-6}
BS	CL-1147	Dissector	S-11	30	0.02	1,000	180 gm	1.5	6.25	E/E	10^{-13}	0	2×10^{-7}	4.6×10^{-6}
TT	FW-146	Dissector	S-1	12	2	3,000		4.5	14	M/M	3×10^{-11}	0	2×10^{-7}	4.8×10^{-6}
TT	FW-118	Dissector	S-1	20	3			2	6.3		10^{-10}	0	2×10^{-7}	
E	8507	Vidicon	S-18	150	0.02	2,000		1.125	6.25	M/M		0.03	0.2	2.1×10^{-4}
E	8541	Vidicon	5500 A (peak)	150	0.02	2,000	2.0 oz	1.125	6.25	M/M		0.03	0.2	2.1×10^{-4}
lachlett	2058G	Vidicon	S-18	1	0.08	2,000	10.0 oz	2.25	12.0	M/M		0.03	1.0	4.8×10^{-4}
CA	8521	Vidicon	5500 A (peak)	35	0.02	1,000		1.6	8.0	M/M		0.03	0.2	3.3×10^{-5}
estinghouse	WX-30152	SEC vid.	S-20	9,000		1,000		2.75	12.4	E/M		0.03	0.3	4.0×10^{-5}
CA	8480	Vidicon		4		1,400		1.6	10.375	E/M		0.03	0.3	3.2×10^{-4}
EC	TD 8484	Vidicon	4800 A (peak)	200	0.02	1,700		1.125	6.250	M/M		0.03	0.2	2.4×10^{-4}
CA	8507	Vidicon	5500 A (peak)	150	0.02	2,000	2.0 oz	1.125	6.250	M/M		0.03	0.2	2.1×10^{-4}

Approved for Release: 2021/12/09 C05137011

SECRET

3.4 TECHNICAL DISCUSSION

3.4.1 Theory of Operation

A vidicon focus sensor is closely related in operation to the vidicon V/h sensor. In the latter, the vidicon camera senses and corrects for scene motion at right angles to the optical axis. In the vidicon focus sensor, the camera senses image defocusing, which is produced by scene or equipment movement along the optical axis.

One of the underlying principles of operation of the vidicon focus sensor is that the time frequency components of the video signal, v(t), are related to the spatial frequency components of the image formed on the vidicon tube. For example, we assume that the vidicon photoconductor is scanned by an electron beam with a standard raster scan to generate v(t). This scanning process "slices" the electronic pattern, formed by the optical image in the photoconductor, into a specified number of horizontal lines. If the horizontal dimension of the photoconductor is L, and time T is required for the beam to scan across one line, then the spatial frequency for this direction, n_X, is related to the video frequency, f, by the following:

$$f = \frac{n_X L}{T}$$

On the other hand, no clear relationship exists between spatial frequencies of the vertical dimension, called n_Y, and the video components because the video waveform can only be related to one dimension although the image has two dimensions.

Since the image spectrum can be related to the video spectrum in at least one dimension, an attenuation of spatial frequency components in the image produces a corresponding attenuation of video frequency components. This attenuation notably occurs when the image is defocused. Here we interject the fact that the average power of the video signal, P_{ave}, is related to the spectrum of v(t). Therefore, we can measure the degree of image defocusing by measuring the average power of v(t). When the image is in best focus on the vidicon tube, P_{ave} is a maximum. As the image is progressively defocused, P_{ave} decreases monotonically from its maximum value. This is another underlying principle of operation of the vidicon focus sensor.

In the V/h sensor, the average power of the video signal is proportional to image motion. In order to convey this information in an easily handled form for closed loop control, the image is sinusoidally wobbled on the vidicon tube. Due to the storage property of the photoconductor, the stored image is alternately blurred and resolved by such wobbling. Thus, the average power is modulated. If there is no image motion produced by scene motion, the modulation is balanced. If there is scene motion, the resulting modulation is unbalanced, which is necessary for generating an error correcting signal. The parallel of this system for focus control using a vidicon focus sensor is obvious. In fact, the only major different component in the two systems is the optical modulating element. In such an automatic focus control system, the modulating element must alternately focus and defocus the image on the vidicon tube. Nevertheless, the same electronic detection and processing circuitry can be used in each system, with only minor changes in components.

3.4.2 Parametric Analysis

3.4.2.1 Focus Requirements

A design goal of ±0.0005 inch was set as the error between true focus position and the focus sensor carriage position.

3.4.2.2 Test Scene Requirements

The test scene was chosen such that it will not limit the focus sensor resolution, i.e., any limitation will be in the focus sensor system. One requirement is that the real scene image at the camera have a scale of 100,000 to 1, minimum. The scene used has a scale of 10,000 to 1; the optics gives a reduction of 12, yielding a total scale of 120,000 to 1.

In addition, the scene has a spatial frequency of at least 50 cycles per millimeter.

3.4.2.3 Camera

The vidicon camera is required to sense 25 cycles per millimeter spatial frequency content of the real scene. This requires 1,000 TV lines and a minimum bandwidth of 10 megacycles for the standard horizontal sweep frequency, 525-line raster.

3.4.2.4 Alignment Tolerances

Alignment tolerances of the vidicon photosensitive surface, the lens optical axis, and the line of sight are required to be perpendicular or parallel to each other to better than 1 minute of arc. Alignments were achieved at approximately 1/2 minute of arc.

Real scene position is not critical and may be positioned to within 1/8 inch.

3.4.2.5 Video Electronics

High-Pass Filter and Video Amplifier

The specifications for the high-pass filter and video amplifier are as follows:

1.	Bandwidth	1 Mhz to 50 Mhz +0, -3 decibels 100 hz to 0.7 Mhz - 40 decibel, minimum
2.	Gain	30 decibel overall
3.	Z in	50 ohms resistive (VSWR < 1.2)
4.	NF	< 8 decibels

Envelope Detector

The envelope detector specifications are as follows:

1.	Type	Peak to peak average power
2.	Threshold	Linear response above 100 millivolts rms input
3.	Loss	6 decibels
4.	Z out	10 kilohms

Integrator

The integrator specifications are as follows:

1.	Time constant	100 milliseconds (equal charge and discharge)
2.	Impedance	20 K ohms

Narrow Band Amplifier

The narrow band amplifier specifications are as follows:

1.	Bandwidith	0.1 hz to 10 hz +0, -0.5 decibels
2.	Gain	40 decibels
3.	Z in	> 20 K ohms
4.	Z out	< 1 K ohms

Synchronous Detector

The specifications for the synchronous detector are as follows:

1.	Type	Full wave, no transformer
2.	Loss	No loss in power

3.4.2.6 Modulation Servo

The primary requirement of the modulation servo is that it provides modulation accuracy consistent with the focus performance to be evaluated and variable in frequency from 0.1 to 10 hertz and in amplitude from 0 to ±10 thousandths of an inch. Fig. 3-4 is a mathematical block diagram of the modulation servo. The symbol definitions are as follows:

K_1 = preamplifier gain
K_2 = power amplifier gain
K_m = motor torque constant
K_3 = lead screw pitch ratio
K_4 = LVDT and LVDT amplifier gain = 100 volts/inch
K_5 = tachometer generator constant
J = moment of inertia referred to motor shaft
CF = shaft coulomb friction
E_m = modulation command signal
Ed = drift referred to input
Td = coulomb friction - induced disturbing torque
ω_m = lead screw rotational rate
x_m = modulation carriage position

The coulomb friction force on the lead screw is about 5 inch-ounces. For position control of 10^{-4} inch resolution, this stiffness is:

$$K_S = K_1 K_2 K_m K_4 = 5 \times 10^4 \frac{\text{in.-oz}}{\text{in.}}$$

$$K_3 = 4 \times 10^{-3} \text{ in./rad}$$

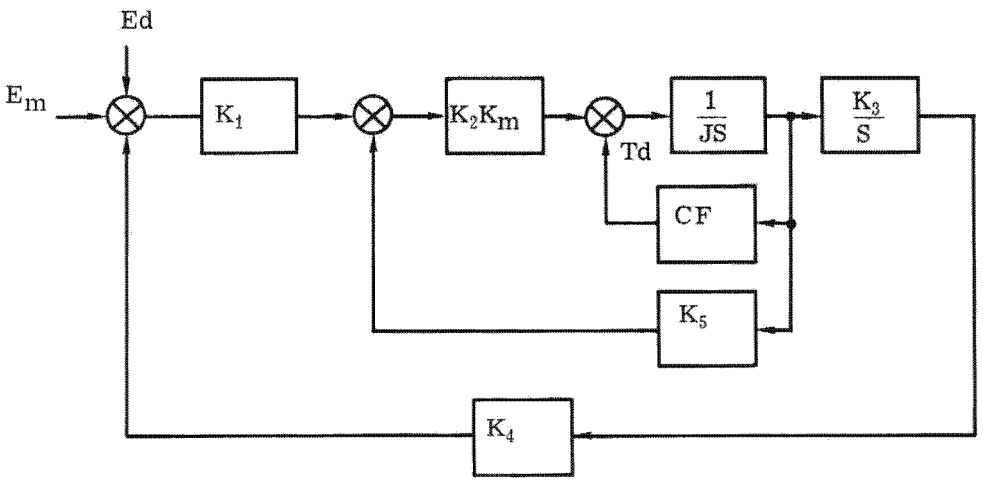

Fig. 3-4 — Modulation servo mathematical block diagram

Also, for a maximum carriage acceleration of 0.10 in./sec^2, motor shaft acceleration of 125 rad/sec^2 is required. Since the maximum torque available is 15 inch-ounces, the inertia wheel moment is 0.12 in.-oz-sec^2. Designing for an inner loop velocity constant (Kvi) of 400 sec^{-1}, the loop damping becomes:

$$\frac{Ks}{Kvi} = \text{damping} = 25\ \frac{\text{in.-oz}}{\text{in./sec}}$$

Therefore, the outer loop velocity constant (Kv_o) is:

$$Kv_o = \frac{K_c\ K_D\ K_o\ K_g}{K_f\ K_e} = \frac{K_g\ K_s}{J\ Kvi} = 0.166\ \text{sec}^{-1}$$

Using $K_f = 10$

$$K_A = \frac{Kvi\ J}{K_m K_f K_e} = 48\ \text{amps/volt}$$

The Bode plot for the inner loop shows that with $\tau_1 = 0.2$ second and $\tau_2 = 0.05$ second, crossover at 100 cps can be achieved with a 60-degree phase margin. Then

$$K_o = Kv = \frac{K_1\ K_c}{K_c\ K_D\ K_g} = 0.21$$

3.4.2.7 Sensor Control Loop

Fig. 3-5 is a mathematical block diagram of the closed sensor control loop. The symbols have the following definitions:

KcKd = camera demodulator gain
K_g = motor-carriage drive ratio
K_o = DC preamp gain
K_A = power amplifier gain
K_m = motor torque constant
K_e = LVDT gain
K_f = LVDT preamp gain
J = system moment of inertia, referred to motor shaft
T_1, T_2 = compensation time constants
CF = coulomb friction force referred to motor shaft
X_o = reference position (best focus)
X_c = carriage position
Φ = camera noise power spectrum
E_d = amplifier drift, referred to demodulator output

Design limits are based upon the resolution required and the acceleration capability of the drive. The drive mechanism consists of a 5:1 spur gear train driving the lead screw. Coulomb friction force at the lead screw is 5 ounces per inch. Therefore, for a resolution of 10^{-4} inch, the stiffness, K_s, at the motor shaft is presented in the following equation.

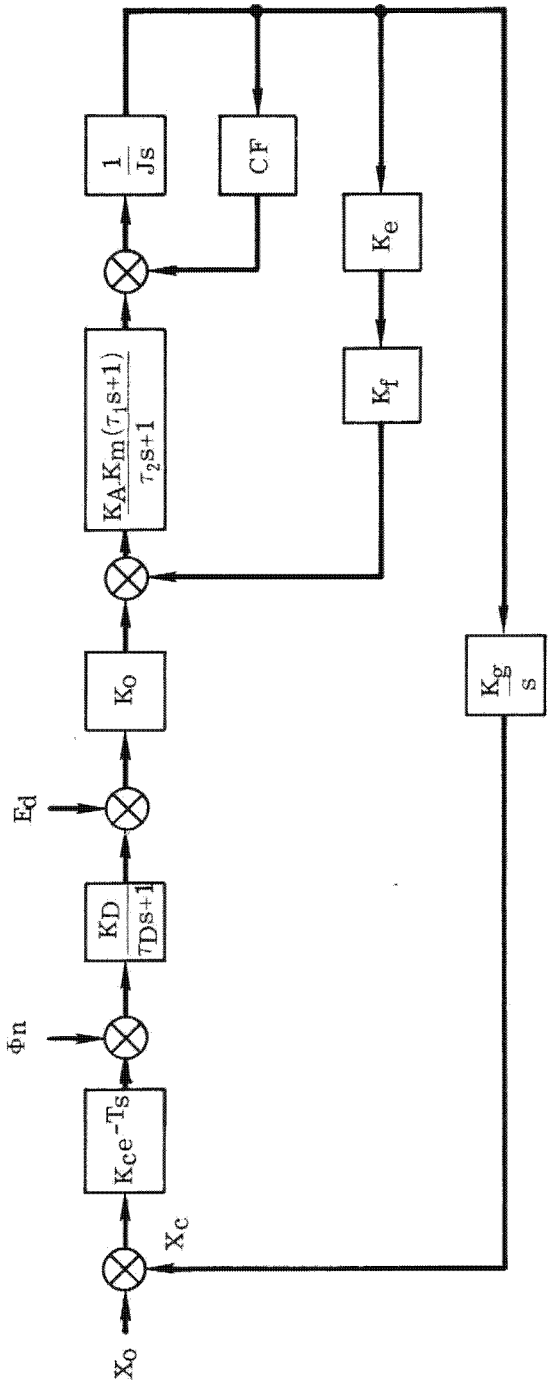

Fig. 3-5 — Mathematical block diagram of the closed sensor control loop

$$K_S = K_C\ K_D\ K_O\ K_a\ K_m = 10^4\ \frac{\text{in.-oz.}}{\text{in.}}$$

3.4.3 Equipment Design

All electronic elements in the system are designed to take advantage of subminiaturization techniques; wherever feasible, hybrid or integrated microcircuits are used. All designs have been produced with an airborne equipment specification design goal, although no environmental testing has been done.

3.4.3.1 Camera

The camera is a Granger Association Model V-1000 vidicon camera, with 1,000-line resolution on a standard commercial raster (525 lines interlaced).

The camera output is a composite video signal, containing in addition to 35 megahertz bandwidth video, a pedestal, line and frame sync, and blanking. The video level from a nominal 1 f.c. scene is 500 millivolts rms at 50 ohms.

3.4.3.2 Test Scene

A variety of scenes involving resolution charts and bar transparencies were used in measuring video component performance.

For focus detection measurement, two scenes were used: a pseudo-random scene, and a real aerial photograph.

The pseudo-random scene is Art-type 4082, a high contrast maze-like form containing high spatial frequencies.

The real scene is a transparency prepared from a high altitude photograph of an airfield. The photograph has been enlarged so that a realistic test for the lens in use is made.

The scene is illuminated by the diffused output of a 300-watt projection lamp operated from a regulated dc supply.

3.4.3.3 Video Processing Electronics

The video processing includes a high-pass filter, a video amplifier and detector, a notch and low-pass filter, a narrow band amplifier, a synchronous demodulator, and an integrator.

High-Pass Filter

The high-pass filter is a three-section Tchebyscheff filter with a corner frequecy of 1 megahertz and minimum 40-decibel rejection of all frequencies below 0.5 megahertz. The filter has input and output impedances of 50 ohms.

Video Amplifier and Detector

The video amplifier consists of two integrated video amplifiers, Amelco Type E13-511, with an overall feedback loop to control gain. The frequency response is -6 decibel per octave below 200 kilohertz, controlled by coupling capacitor values, and is flat ±0.25 decibel from 0.5 megahertz to above 50 megahertz. The circuit exhibits adequate stability and performance to guarantee operation over a wide variety of gain/bandwidth parameters, controlled by the 18K-ohm feedback resistor.

The detector is a peak-to-peak averaging detector, using two-point contact silicon microwave detector diodes. The detector has square law response (linear volts output divided by power input) up to 50 millivolts rms input, and is linear ±2 percent (linear volts output divided by power input) above 100 millivolts rms input. A 20 K-ohm dc return is provided for proper operation of the following low-pass filter.

Notch and Low Pass Filter

A notch filter is required to remove a large 60 hertz p.r.f. blanking signal. This is accomplished by a twin-tee circuit of more than 40-decibel rejection at 60 hertz. A low-pass filter with a 20-millisecond time constant removes video frequency fluctuations from the detector output.

Narrow Band Amplifier

The modulation signal from the detector is amplified by 40 decibels by an amplifier having a 0.1- to 10-hertz response. The amplifier is an Amelco Type A13-251 integrated operational amplifier with 0.1-hertz high-pass input and output coupling, and 10 hertz high-pass negative feedback. The amplifier has constant phase shift (within 5 degrees) in its passband, and 6 decibels per octave rolloff on either end.

Synchronous Demodulator

Synchronous demodulation is accomplished by two field effect transistor gates, driven out of phase. Hybrid circuits containing f.e.t., drive transistor, and diode are used. The gate outputs, representing positive and negative signal halves, are differentially added in an integrated operational amplifier that has a gain of 20 decibels and low-pass filters to remove common mode modulation frequency input.

The demodulator reference drive is derived from the carriage position transducer, where it is present as a low level signal of variable waveform.

Integrator

The integrator provides time constants of 1, 2, 4 or 8 seconds in an operational amplifier with a capacitive feedback. The operational amplifier is followed by a variable resistor to adjust overall feedback loop gain.

3.4.3.4 Modulator

The modulator servo electronics consist of an operational amplifier system, summing input, LVDT and tachometer signals, and a current amplifier.

The low-level LVDT signal is amplified in a Nexus SL-6 amplifier with a closed-loop gain of 11. This signal is added to the modulation input and tachometer input to produce an error signal at a second Nexus SL-6 amplifier; this amplifier has a closed loop gain of 30, with a -6 decibel octave rolloff above 80 hertz.

3.4.3.5 Closed-Loop Sensor

A Nexus SL-6 operational amplifier processes the error signal from the integrator with an inner tachometer loop. The same current amplifier as in paragraph 3.4.3.4 above is used as the torque motor driver.

3.5 EVALUATION OF RESULTS

3.5.1 Static Test Results

Several curves are shown which are representative of static focus measurement data. (Refer to Figs. 3-6 through 3-8.) Each curve plots camera position in thousandths of an inch against millivolts output from the notch and low-pass filter. Fig. 3-9 illustrates the effect of video noise versus time constant in the low-pass filter.

The data shows that a sensitivity of 1 volt per inch can be expected for any illumination above 0.25 foot-candle at vidicon (150 foot-lamberts at scene) and contrasts above 2:1. The measurement error due to drift and random fluctuations is between 0.25 and 0.5 mil. This figure can be reduced in a modulating system because of the use of the steeper portion of the focus detection characteristics, and because of the use of a synchronous demodulation post detection integrator system.

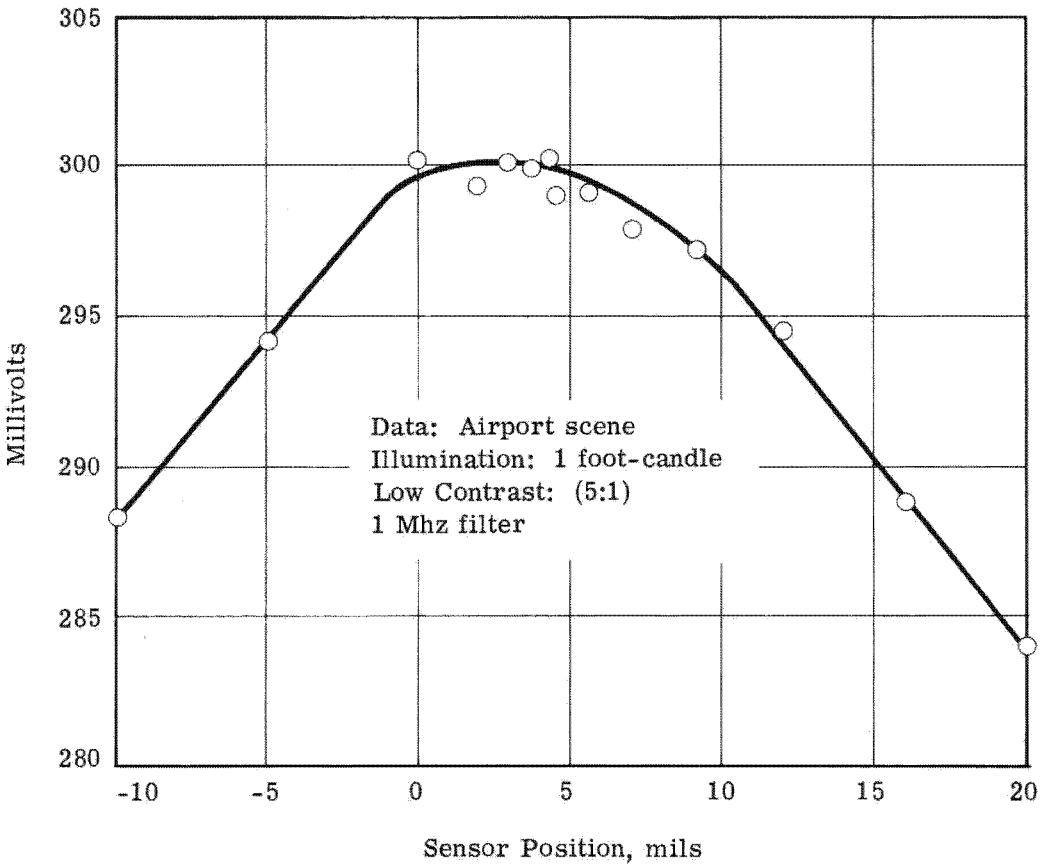

Fig. 3-6 — Camera position versus notch/low-pass filter output, τ = 100 milliseconds

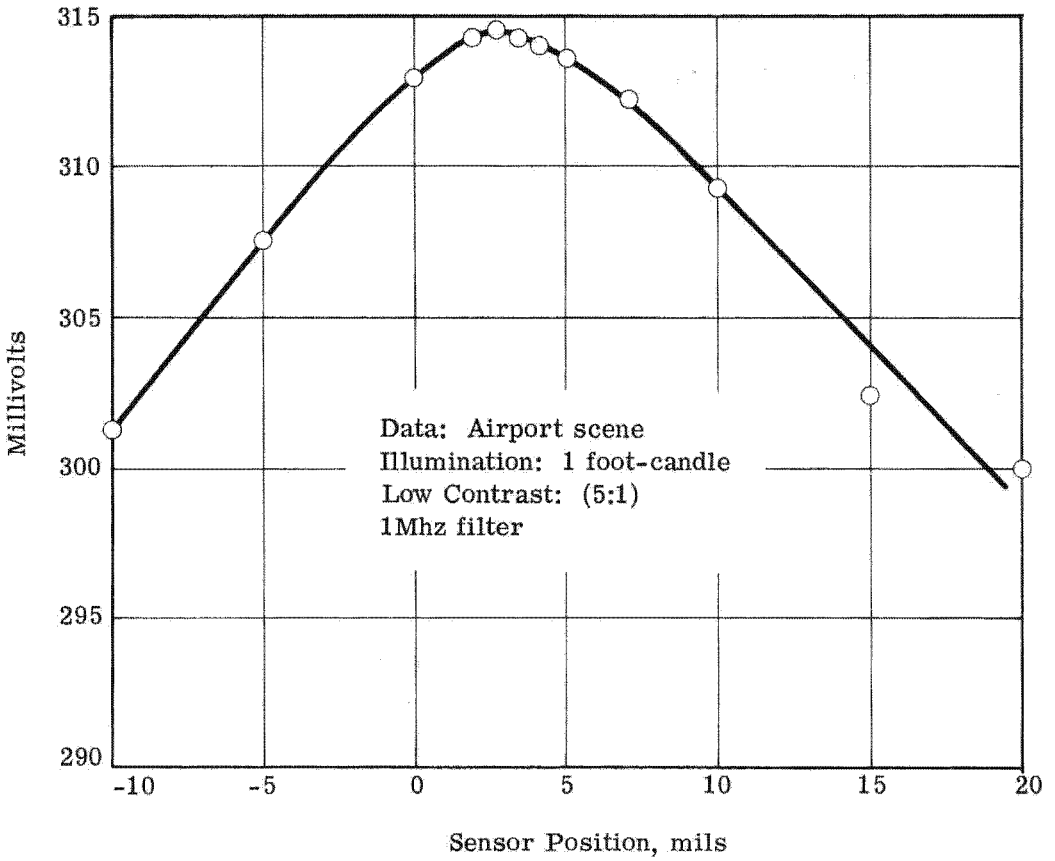

Fig. 3-7 — Camera position versus notch/low-pass filter output, τ = 10 milliseconds

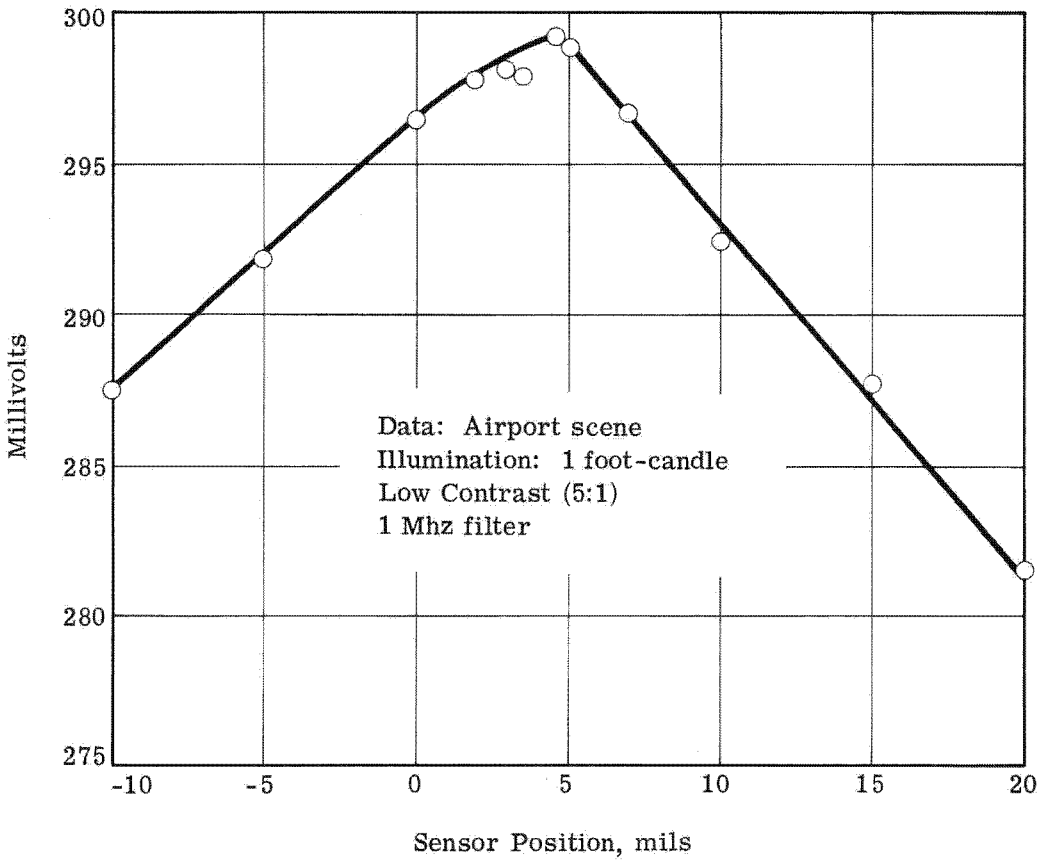

Fig. 3-8 — Camera position versus notch/low-pass filter output, τ = 100 milliseconds (scene rotated 90 degrees)

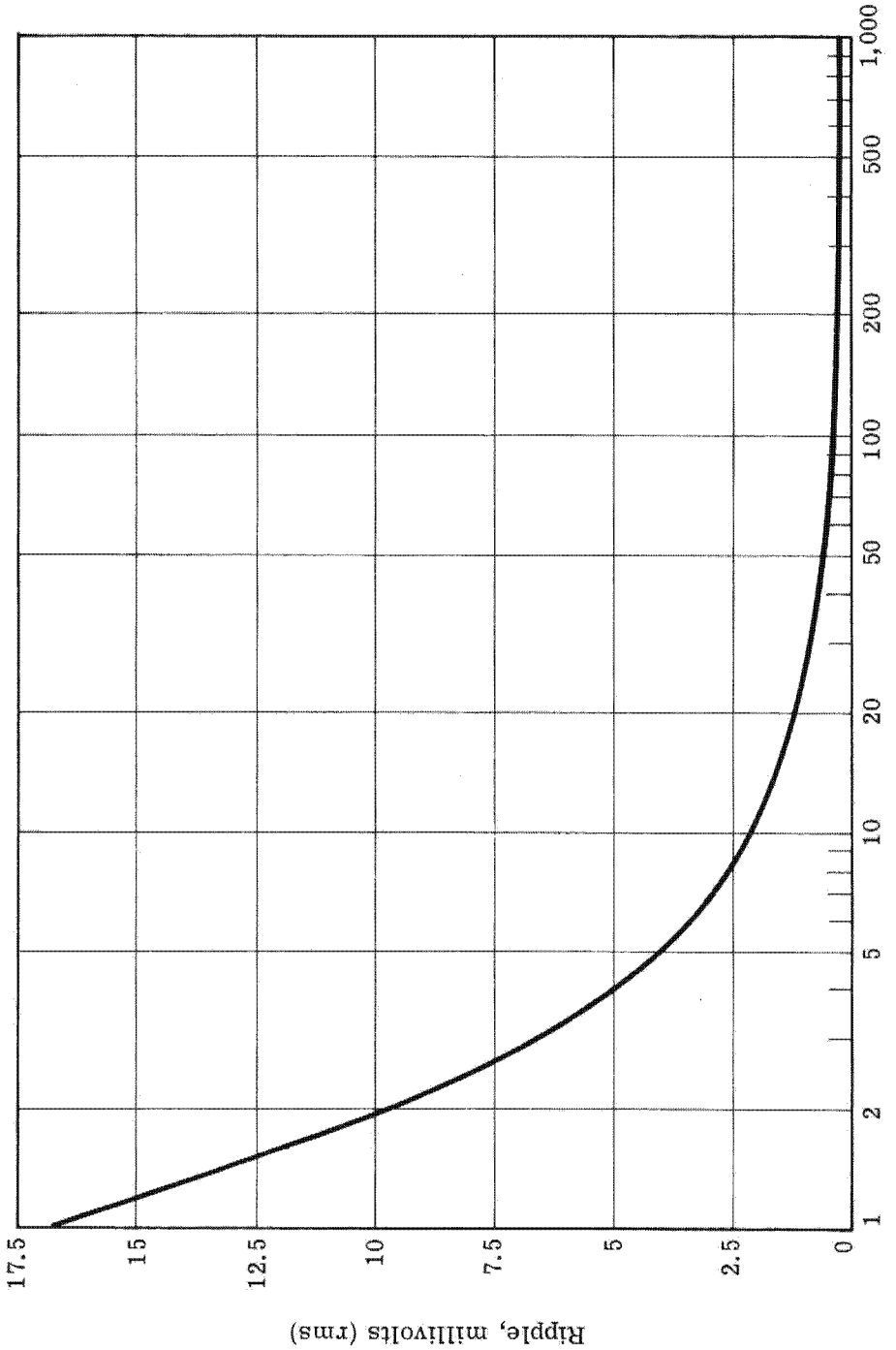

Fig. 3-9 — Video noise versus time constant in the low-pass filter

~~SECRET~~